Title

Angle-resolved photoemission spectroscopy study of the Möbius Kondo insulator candidate CeRhSb

Journal

Physical Review B, 100(3)

ISSN

2469-9950

Authors

Seong, Seungho

Kim, Kyoo

Lee, Eunsook

et al.

Publication Date

2019-07-01

DOI

10.1103/physrevb.100.035121

Peer reviewed

Angle-resolved Photoemission Spectroscopy Study of the Möbius Kondo Insulator Candidate CeRhSb

Seungho Seong[1],* Kyoo Kim[2,3],* Eunsook Lee[1], Chang-Jong Kang[2],† Taesik Nam[2], B. I. Min[2], Takenobu Yoshino[4], T. Takabatake[4], J. D. Denlinger[5],‡ and J.-S. Kang[1]§

[1]*Department of Physics, The Catholic University of Korea, Bucheon 14662, Korea*

[2]*Department of Physics, Pohang University of Science and Technology, Pohang, 37673, Korea*

[3]*MPPHC_CPM, Pohang University of Science and Technology, Pohang 37673, Korea*

[4]*Department of Quantum Matter, Graduate School of Advanced Sciences of Matter, Hiroshima University, Higashi-Hiroshima 739-8530, Japan*

[5]*Advanced Light Source (ALS), Lawrence Berkeley Laboratory, Berkeley, CA. 12345, USA*

The electronic structure of a Möbius Kondo insulator (MKI) candidate of CeRhSb has been investigated by employing angle-resolved photoemission spectroscopy (ARPES), and the density functional theory (DFT) and dynamical mean-field theory (DMFT) band calculations. The Fermi surfaces (FS's) and band structures are successfully measured for three orthogonal crystallographic directions. A sharp Ce $4f$ peak is observed at the Fermi level ($E_{\rm F}$), and its temperature (T)-evolution agrees with that of the Ce $4f$ Kondo resonance. The metallic FS's are obtained for all three different (100), (010), and (001) planes. The Ce $4f$ FS's are described properly by the unfolded DFT calculations considering the reduced Ce-only unit cell. The T-dependence of Ce $4f$ states as well as the dispersive coherent Ce $4f$ bands are described well by the DMFT calculations, and reveal the anisotropic c-f hybridization. The photon energy dependence of the Fermi-edge states in CeRhSb reveals the $3D$ character, consistent with the bulk states dispersing to $E_{\rm F}$ over a larger energy scale rather than the predicted Möbius topological surface states.

PACS numbers: 79.60.-i,71.20.-b,71.27.+a,71.20.Eh

Topological Kondo insulators (TKI's) belong to a class of the symmetry-protected topological phases arising from the effects of strong correlation.[1,2] In TKI's, the temperature (T)-dependent Kondo hybridization between conduction electrons and localized f-electrons leads to the formation of a narrow gap in the bulk bands at the Fermi level ($E_{\rm F}$) and the topologically nontrivial band inversion. The first theoretically-predicted TKI was SmB_6,[1,2] which was known as a mixed-valent (Sm^{2+}/Sm^{3+}) Kondo insulator, but having the resistivity saturation at low T. The metallic surface states have been observed by angle-resolved photoemission spectroscopy (ARPES)[3–6] and transport experiment,[7–10] supporting SmB_6 being a promising candidate for a TKI. But there are conflicting ARPES reports, claiming SmB_6 being just a trivial Kondo insulator.[11,12] Subsequently, other rare-earth f-electron systems, such as YbB_6, YbB_{12}, and g-SmS, were proposed as TKI's or topological Kondo semi-metals.[13–17] Nevertheless, the general consensus on the $4f$-electron TKI's is still lacking.[18]

It has been recently predicted that CeNiSn, CeRhSb, and CeIrSb are novel topological Kondo systems having Möbius-twisted surface states.[19] They belong to the failed Kondo insulators, for which an insulating gap develops due to the Kondo screening and yet a semimetallic phase is stabilized at lower T, exhibiting large anisotropy.[20–22] The f-electron pseudo gaps of size $15-20$ meV were observed at $E_{\rm F}$ in high-resolution PES for CeRhSb[23,24] with a metallic density of states (DOS) at $E_{\rm F}$, supporting a Kondo semi-metallic phase. On the other hand, tiny gaps as small as $\sim$ 28 K ($\sim$ 2.3 meV) and $\sim$ 7 K ($\sim$ 0.6 meV) were reported in NMR[25] and in resistivity experiments,[26] respectively.

The unique features of these systems are the nonsymmorphic glide and screw axis symmetries (*Pnma* space group) (see Fig. 1), which bring about the hourglass-type new topological surface band structures.[19] Hence these systems are called the Möbius Kondo Insulators (MKI's). But the predicted features of the MKI's have not been confirmed experimentally yet.

In this work, we have studied the electronic structures of a candidate MKI, CeRhSb, employing both ARPES experiment and the density functional theory (DFT) and dynamical mean-field theory (DMFT) band calculations. We have successfully measured Fermi surfaces (FS's) and band structures for the three orthogonal crystallographic directions. This is important because theoretically the Möbius surface states are predicted only for the (010) surface, while the (100) surface is predicted to be insulating.[19] We have also performed T-dependent ARPES measurement, and observed dramatic k-shifting in the Ce $4f$ peak near $E_{\rm F}$, which allows us to estimate the coherence temperature, T_{coh}, of Ce $4f$ states.

Single-crystalline CeRhSb samples were prepared by the Bridgman method.[22] They were characterized to be of very good quality and exhibited strong anisotropy in thermal conductivity. The details of the sample preparation and characterization are described in Ref.[22]. According to the X-ray analysis, the lattice constants are a=7.47 Å, b=4.63 Å, and c=7.89 Å.

ARPES measurements were carried out at the MERLIN beamline 4.0.3 at the Advanced Light Source (ALS) synchrotron. Single crystalline samples were cleaved *in situ* using a blade-type cleaver,[27] and measured in vac-

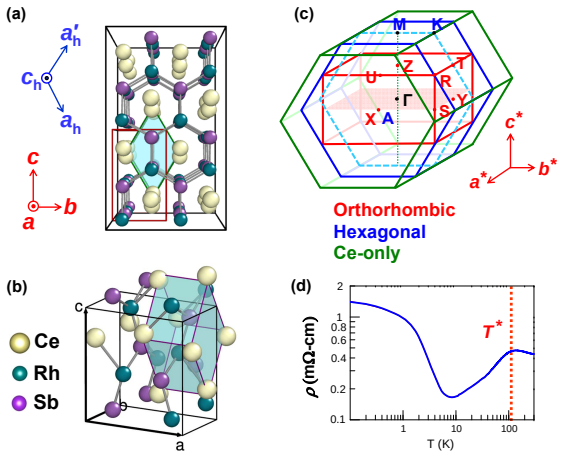

FIG. 1: (Color online) Crystal structure and BZ of CeRhSb. (a) The orthorhombic ϵ-TiNiSi-type structure viewed from the [100] direction, showing that the orthorhombic structure is slightly deformed from the hexagonal structure. (b) The original unit cell (black lines) versus the reduced Ce-only unit cell (the blue-colored cell), for which only Ce ions are considered and Rh and Sb ions are ignored. (c) The BZ's of the orthorhombic (red), hexagonal (blue), and Ce-only (green) structures, superposed onto one another. (d) The resistivity $\rho(T)$ for polycrystalline CeRhSb (adapted from Ref.[38]).

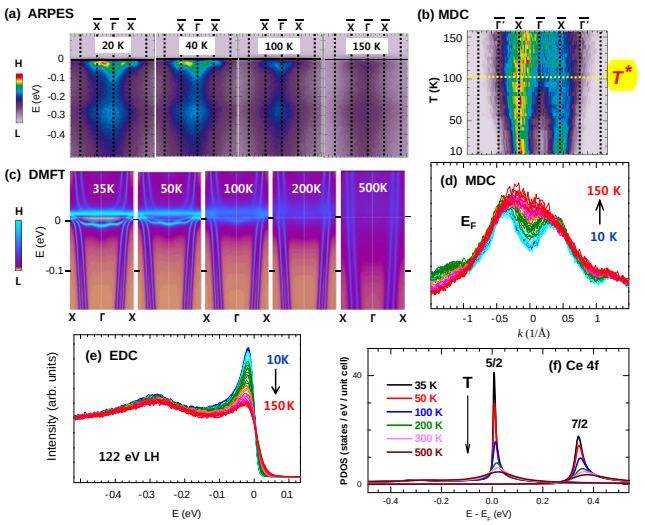

FIG. 2: (Color online) T-dependent $4f$ states of CeRhSb. All the ARPES data are obtained at the Ce $4f$ resonance ($h\nu$=122 eV) and normalized to the maximum intensity at each T. (a) The ARPES images along $\bar{X}\bar{\Gamma}\bar{X}$ for selected temperatures. (b) The normalized MDC images of the Fermi-edge states along $\bar{X}\bar{\Gamma}\bar{X}$ from 10 K to 150 K. (c) The calculated T-dependent DMFT band structures. (d) The E_F-intensity profile of the MDC's along $\bar{X}\bar{\Gamma}\bar{X}$ from 10 K to 150 K. (f) The calculated T-dependent variation of the Ce $4f$ PDOS, obtained in the DMFT.

uum better than 5×10^{-11} Torr and at $T\sim20$ K with further cooling to 6 K during T-dependent measurements. Fermi level (E_F) energy referencing was performed with evaporated gold. A total energy resolution of $\Delta E\approx25$ meV was employed at 122 eV photon energy, and the detector 0.1° angular resolution translates to momentum resolution of $\Delta k<0.01$ Å^{-1} at 122 eV. Notable is that the energy resolution of the ARPES data is limited by non-ideally-flat surfaces of CeRhSb,[27] as described in Fig. S1 in the supplement. FS maps were obtained via polar scans of the sample. In plotting FS maps, the energy window of $E_i\pm16$ meV was integrated.[28] Photon energies corresponding to the high-symmetry planes were determined from the photon energy ($h\nu$) scans.[29]

We have calculated the electronic structure of CeRhSb within the DFT using the full-potential local-orbital band method (FPLO) in the generalized-gradient approximation.[30] To describe the band structures in an effectively reduced unit cell, we have utilized the band unfolding scheme[31] implemented in the FPLO code. To describe the strong electron correlation effect of the Ce $4f$ state in the Kondo coherence regime, we have utilized the DFT+DMFT method implemented in the Wien2k code.[32,33] One-crossing approximation (OCA) was used for the DMFT impurity solver.[34] The on-site Coulomb U=5.5 eV and Hund's coupling J= 0.68 eV for the Ce $4f$ electrons were adopted in the DMFT calculation.

Figure 1(a) shows a view from the [100] direction in the ϵ-TiNiSi-type orthorhombic structure of CeRhSb.[35] CeRhSb has an AlB_2-derivative structure (Al=Ce, B=Rh, Sb) having a subcell with Rh and Sb atoms on the hexagons.[36] The orthorhombic structure of CeRhSb is slightly deformed from the hexagonal structure, for which the a-axis in the orthorhombic structure corresponds to the c_h-axis in the hexagonal structure.[37] Ce atoms form a zigzag chain along a (c_h).[37] Hence large anisotropic physical properties are expected to originate from the Ce chains along a (along c_h in the hexagonal structure) in CeRhSb, in agreement with the reported properties.[20–22] Figures 1(b) and (c) show the original versus the Ce-only reduced unit cells, and the Brillouin zones (BZ's) of the orthorhombic, hexagonal, and Ce-only structures, superposed onto one other, respectively. The Γ-X, Γ-Z, and Γ-Y lines in the orthorhombic BZ are along the Γ-A, Γ-M, and Γ-K lines in the hexagonal BZ.

Figure 1(d) shows the resistivity $\rho(T)$ for polycrystalline CeRhSb, reproduced from Ref.[38]. It exhibits a typical $\rho(T)$ behavior of a Kondo insulator, having a hump and dip structure at $T^*\approx100$ K and $T\approx10$ K, respectively.[16] At very low T, it shows a hint of the plateau-like behavior. A similar behavior was observed in Ref.[26]

The Kondo-like temperature evolution of the f-states in CeRhSb along $\bar{X}\bar{\Gamma}\bar{X}$ for the (001) surface is presented in Fig. 2, measured at the Ce $4f$ resonance ($h\nu$=122 eV) using linear horizontal (LH) polarization. The ARPES images for selected temperatures of this data set are shown in Fig. 2(a), exhibiting two separated strong Fermi-edge peaks on either side of normal emission ($\bar{\Gamma}$). With increasing T, the f-amplitudes decrease, the k-gap

re-ordered text discussion to match re-ordered panels in Fig. 2 (a), (b) & (d), (e), (c) & (f)

(e) & (f) repeat the same FS map just to show different cut direction

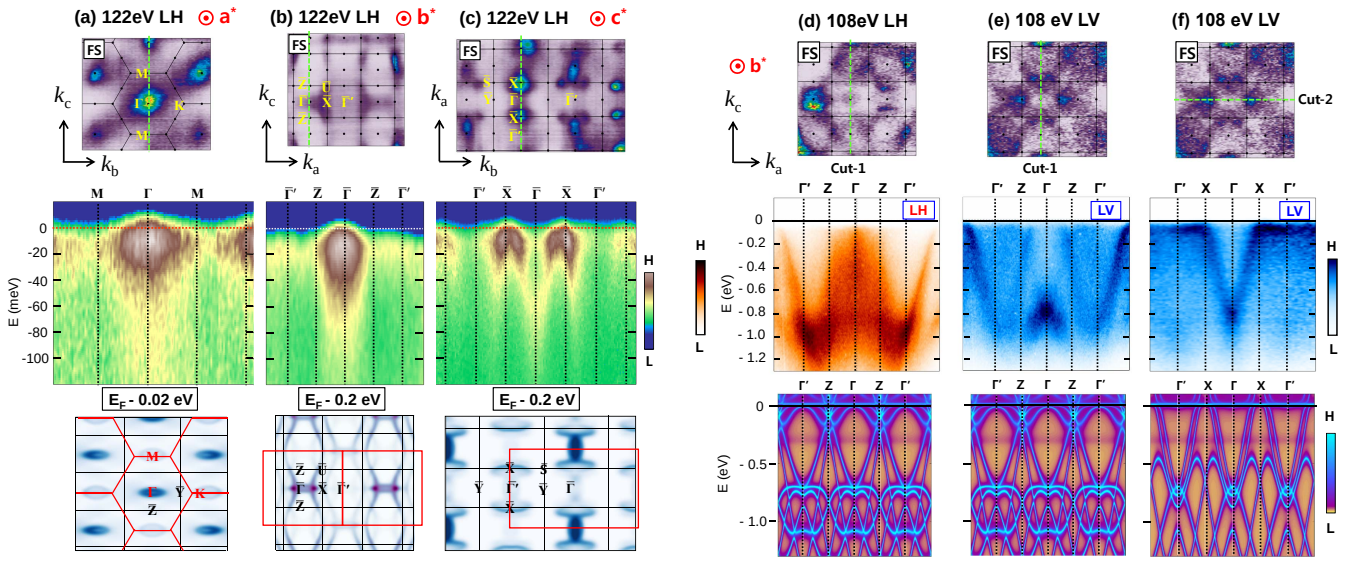

FIG. 3: (Color online) (a)-(c) Fermi surfaces (FS's) and ARPES data obtained at the Ce $4f$ resonance ($h\nu$=122 eV)[29] and at T=20 K with the LH polarization, and the DFT-calculated FS's of CeRhSb for three orthogonal planes, respectively. In the top panel are shown the measured FS's for the (100) plane, the (010) plane, and the (001) plane, respectively. In the middle panel are shown the measured ARPES spectra along the several cuts, denoted as green dotted lines in the FS's of top panel. The bottom panel presents the DFT-calculated FS's,[40] which are unfolded into a larger hexagonal BZ (in red) of the Ce-only unit cell. The original orthorhombic BZ's are denoted in black. (d)-(f) FS's and ARPESs of CeRhSb for the (010) plane obtained at T=20 K with $h\nu$=108 eV,[29] and the corresponding DMFT band structures calculated at T=50 K. (d) ARPES along $\Gamma' Z \Gamma Z \Gamma'$ (Cut-1) (denoted as green dotted lines in the FS of top panel), obtained with the LH-polarization, is compared with the DMFT band structure at the bottom. (e),(f) Similarly for two ARPESs along $\Gamma' Z \Gamma Z \Gamma'$ (Cut-1) and along $\Gamma' X \Gamma X \Gamma'$ (Cut-2), respectively, both of which are obtained with the LV-polarization.

between the two E_F-peaks disappears, and the two peaks merge into a single central peak at k=0. This behavior is highlighted by plotting the Fermi-edge momentum distribution curves (MDC) both as a normalized image in Fig. 2(b) and as the line cuts in Fig. 2(d). The T-dependent variation of the Fermi-edge states manifests that, upon heating, the sharp peaks merge into one peak at $T^*\sim$100 K, indicating that the coherent Ce $4f$ band along $\bar{\Gamma}$-$\bar{X}$ is formed below T^*, suggesting $T_{coh} \approx T^* \approx 100$ K. Figure 2(e) shows the full T-series of the angle-integrated energy distribution curve (EDC) spectra, which highlights the energy, width, and amplitude variation of the resonantly enhanced f-character Kondo peak near E_F. The additional broad feature at -0.3 eV represents a final-state spin-orbit (SO) side band peak. With increasing T, the intensity of the Kondo peak decreases dramatically with the concomitant broadening of its energy width.

The T-dependent variations of the DMFT band structure and the Ce $4f$ partial density of states (PDOS) are shown in Figs. 2(c) and (f), respectively. Upon cooling below $T\approx$100 K, the Ce $4f$ Kondo-resonance band near E_F and the flat SO side bands at $\sim \pm 0.3$ eV are formed (see Fig. S4 in the supplement), in agreement with ARPES measurement. The SO side band above E_F is more pronounced than that below E_F. In fact, this T-evolution behavior of CeRhSb both in ARPES and DMFT is consistent with its $\rho(T)$ behavior, having a maximum at $T^*\approx$100 K (see also Fig. 1(a)).[26,38]

Figures 3(a)-(c) show the measured FS's and ARPES spectra, obtained at the Ce $4f$ resonance, and the DFT-calculated FS's of CeRhSb for three different planes. The FS's in the top panel reveal clearly the six-fold symmetry for the (100) plane, the nearly four-fold symmetry for the (010) plane, and the two-fold symmetry for the (001) plane, which support the relation between the orthorhombic and hexagonal structures, described in Fig. 1. The Laue patterns, obtained after ARPES measurements, confirmed the same symmetries as the measured FS's (see Fig. S1 in the supplement).[39] These FS's reflect that all (100), (010), (001) surfaces are metallic. The (100) plane exhibits the circular FS's around Γ points of the hexagonal BZ, while the (010) plane exhibits rather large elliptical FS's and the (001) plane reveals the complicated FS's of polka-dot patterns. Unlike the theoretical prediction,[19] no gap is quantified in the (100) plane in our ARPES.

The FS's and ARPES bands in Fig. 3(a)-(c) arise from the Kondo resonance states. The measured FS's in the (010) plane are larger than the size of the orthorhombic BZ, but appear to fit in with the enlarged BZ's, implying the reduced unit cell. This strange feature arises from the fact that these FS's originate from Ce $4f$ electrons. Indeed, such a reduced unit cell can be obtained when considering Ce atoms only but ignoring Rh and Sb atoms

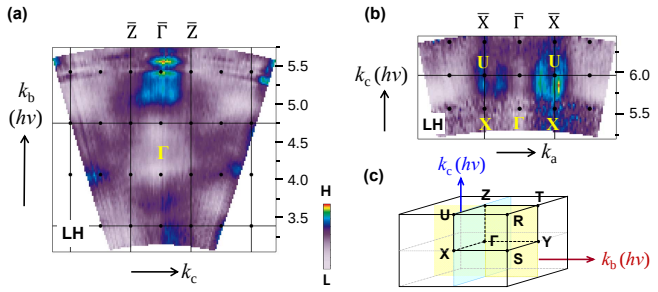

FIG. 4: (Color online) The Fermi-edge state $h\nu$-maps, (a) between 30 eV and 118 eV with $h\nu$ along k_b, and (b) between 100 eV and 150 eV with $h\nu$ along k_c. Both are obtained with the LH-polarization. (c) The $3D$ orthorhombic BZ for which $h\nu$-maps are obtained: the k_c-k_b (yellow) and k_a-k_c (blue) planes for (a) and (b), respectively.

(see Fig. 1 and Fig. S2 in the supplement).[39] Since the FS's in Fig. 3(a)-(c) were obtained at the Ce resonance, they are dominated by Ce $4f$ electrons, and the contributions from Rh $4d$ and Sb $5p$ electrons are negligibly weak.[41] This interpretation is supported by the smaller sizes of the FS, obtained away from the Ce $4f$ resonance ($h\nu$=108 eV) (see Fig. 3(d)-(f)), in which the Rh $4d$ electron contribution is large.

The measured Ce $4f$ states along $\bar{X}\bar{\Gamma}\bar{X}$ in the (001) plane (in Fig. 3(c)) show the hole-like FS pockets around $\bar{X}$ and an electron-like pocket around $\bar{\Gamma}$. They are more dispersive than those along $M\Gamma M$ in Fig. 3(a) and along $\bar{Z}\bar{\Gamma}\bar{Z}$ in Fig. 3(b).[29] The dispersive Ce $4f$ states along $\bar{X}\bar{\Gamma}\bar{X}$ originate from the zigzag Ce chain along [100]. In fact, the DMFT calculation at T=50 K also shows the almost coherent Ce $4f$ band at E_F, revealing the formation of hybridization gap. The DMFT band structures of CeRhSb in the whole BZ, given in Fig. S4 of the supplement,[39] show the coherent Ce $4f$ Kondo-resonance band near E_F and the flat SO side bands at around $\pm$0.3 eV. The observed band slopes indicate the larger effective mass along $M\Gamma M$ and $\bar{Z}\bar{\Gamma}\bar{Z}$, while a smaller effective mass along $\bar{X}\bar{\Gamma}\bar{X}$. Such differences reflect the anisotropic c-f hybridization (c: conduction electron) along different k directions, in agreement with the observed anisotropic properties.[20,22]

The DFT-calculated FS's in the bottom panel of Figs. 3(a)-(c) represent those unfolded into the larger BZ of the reduced Ce-only unit cell.[39] It is noteworthy that the low-T electronic structures and their FS's of strongly-correlated f-electron systems are simulated well by the renormalized DFT bands.[16,34] Indeed, the comparison between the measured FS's and the calculated FS's reveals fairly good agreement. Especially, the FS for the (100) plane in Fig. 3(a), exhibiting the hexagonal-like symmetry, is described fairly well by the FS unfolded into the larger hexagonal BZ (in red) of Ce-only unit cell. Further, the spectral weights of the FS's for the (010) and (001) planes (in Figs. 3(b) and (c)) match well with the periodicity of the Ce-only BZ, as shown at the bottom panels.

Figures 3(d)-(f) show the comparison between the measured ARPES data, obtained with $h\nu$=108 eV,[29] and the DMFT bands calculated at T=50 K for CeRhSb. Note that, in the ARPES with $h\nu$=108 eV, Rh $4d$ states are observed significantly. In Fig. 3(d) are compared the ARPES image plot along $\Gamma' Z \Gamma Z \Gamma'$, obtained with the LH polarization, with the DMFT-calculated bands along the same direction. Similarly, the ARPES image plots along $\Gamma' Z \Gamma Z \Gamma'$ and $\Gamma' X \Gamma X \Gamma'$, obtained with the linear-vertical (LV)-polarized photons, are compared with the corresponding DMFT-calculated bands in Figs. 3(e) and (f), respectively. Excluding the flat Ce $4f$ states in DMFT, they reveal reasonably good agreement. Both the shapes and energy positions of the measured Rh bands agree well with those in the calculated DMFT.[42]

In order to check whether the metallic states, observed in our ARPES, have the $2D$ topological surface-state (TSS) character, we have measured the $h\nu$-dependence of the Fermi-edge states for CeRhSb (called the $h\nu$-map hereafter). Figures 4(a) and (b) show the Fermi-edge state $h\nu$-map, obtained between 30 eV and 118 eV with $h\nu$ along k_b, and that between 100 eV and 150 eV with $h\nu$ along k_c, respectively. The $h\nu$ map in the k_b-k_c plane exhibits the elliptical FS's and the roughly two-fold symmetry, while that in the k_a-k_c plane exhibits the hole-like FS's[44] around U points, providing evidence for the $3D$ character of the Fermi-edge states in CeRhSb. Namely, the theoretically predicted TSS's of the $2D$ character[19] are not observed. This finding does not rule out the possible MKI of CeRhSb, because it may be due to the lack of the ARPES energy resolution relative to the small gap size. Nevertheless, the $3D$ character of the metallic states observed in Fig. 4 indicates that only the pseudo gap opens in CeRhSb, with the gap size $\lesssim$ 20 meV, which is consistent with the earlier high-resolution PES[23,24] and tunneling studies.[21] Therefore, this work suggests that a crucial factor for the realization of the existence of the TSS in a potential MKI is the full bulk insulating energy gap on top of the non-symmorphic crystal symmetries. In this respect, the isostructural CeRhAs, which possesses the full bulk energy gap, would be more appropriate to explore the TSS of MKI.

In conclusion, we have successfully measured the FS's and band structures of an MKI candidate CeRhSb for the three orthogonal crystallographic directions. A sharp Ce $4f$ peak is observed at E_F and its T-evolution agrees with that of the coherent Ce $4f$ band formation, suggesting $T_{coh} \approx 100$ K. The metallic FS's are obtained for all three different (100), (010), and (001) planes. The Ce $4f$ FS's are described very well by the unfolded DFT calculations considering the reduced Ce-only unit cell. The T-dependence of Ce $4f$ states as well as the dispersive coherent Ce $4f$ bands are described well by the DMFT calculations, and reveal the anisotropic c-f hybridization. The $h\nu$-dependences of the Fermi-edge states reveal their $3D$ metallic character, which is consistent with the bulk states dispersing to E_F over a larger energy scale rather

than the TSS's over the tiny hybridization gap. To make a firm realization of the existence of the TSS's of the MKI, ultralow-T and very high-resolution ARPES experiment is highly desirable, albeit quite challenging due to the intrinsic limitation of the non-ideally flat sample surfaces.[27]

Acknowledgments – This work was supported by the National Research Foundation (NRF) of Korea (No. 2016R1D1A1B03932391; No. 2017M2A2A6A01071297; No. 2017R1A2B4005175), Max-Plank POSTECH/KOREA Research Initiative (No. 2016K1A4A4A01922028), and KISTI (Grant No. KSC-2017-C3-0057). The ALS is supported by US DOE under Contract No. DE-AC02-05CH11231. The travel for the ARPES experiment at the ALS was supported in part by MSIP and PAL in Korea.

---

* Co-first authors: They contributed equally.
† Present address: Department of Physics and Astronomy, Rutgers University, Piscataway, New Jersey, 08854, USA
‡ Co-corresponding: JDDenlinger@lbl.gov
§ Co-corresponding: kangjs@catholic.ac.kr

[1] M. Dzero, K. Sun, V. Galitski, and P. Coleman, Phys. Rev. Lett. **104**, 106408 (2010).
[2] M. Dzero, K. Sun, P. Coleman, and V. Galitski, Phys. Rev. B **85**, 045130 (2012).
[3] M. Neupane, N. Alidoust, S-Y. Xu, T. Kondo, Y. Ishida, D. J. Kim, Chang Liu, I. Belopolski, Y. J. Jo, T-R. Chang, H-T. Jeng, T. Durakiewicz, L. Balicas, H. Lin, A. Bansil, S. Shin, Z. Fisk, and M. Z. Hasan, Nature Commun. **4**, 3991 (2013).
[4] N. Xu, X. Shi, P. K. Biswas, C. E. Matt, R. S. Dhaka, Y. Huang, N. C. Plumb, M. Radović, J. H. Dil, E. Pomjakushina, K. Conder, A. Amato, Z. Salman, D. McK. Paul, J. Mesot, H. Ding, and M. Shi, Phys. Rev. B **88**, 121102 (2013).
[5] J. Jiang, S. Li, T. Zhang, Z. Sun, F. Chen, Z. R. Ye, M. Xu, Q. Q. Ge, S. Y. Tan, X. H. Niu, M. Xia, B. P. Xie, Y. F. Li, X. H. Chen, H. H. Wen, and D. L. Feng Nature Commun. **4**, 4010 (2013).
[6] J. D. Denlinger, J. W. Allen, J.-S. Kang, K. Sun, J.-W. Kim, J. H. Shim, B. I. Min, Dae-Jeong Kim, Z. Fisk, arXiv: 1312.6637 (2013).
[7] S. Wolgast, C. Kurdak, K. Sun, J. W. Allen, D.-J. Kim, and Z. Fisk, Phys. Rev. B **88**, 180405 (2013).
[8] D. J. Kim, S. Thomas, T. Grant, J. Botimer, Z. Fisk, and Jing Xia, Sci. Rep. **3**, 3150 (2013).
[9] D. J. Kim, J. Xia, and Z. Fisk, Nature Mater. **13**, 466 (2014).
[10] S. Thomas, D. J. Kim, S. B. Chung, T. Grant, Z. Fisk, and Jing Xia, arXiv: 1307.4133 (2013).
[11] Z.-H. Zhu, A. Nicolaou, G. Levy, N. P. Butch, P. Syers, X. F. Wang, J. Paglione, G. A. Sawatzky, I. S. Elfimov, and A. Damascelli, Phys. Rev. Lett. **111**, 216402 (2013).
[12] P. Hlawenka, K. Siemensmeyer, E. Weschke, A. Varykhalov, J. Sánchez-Barriga, N. Y. Shitsevalova, A. V. Dukhnenko, V. B. Filipov, S. Gabáni, K. Flachbart, O. Rader, and E. D. L. Rienks, Nat. Commun. **9**, 517 (2018).
[13] B. Yan, L. Muchler, X.-L. Qi, S.-C. Zhang, and C. Felser, Phys. Rev. B **85**, 165125 (2012).
[14] X. Zhang, H. Zhang, J. Wang, C. Felser, S.-C. Zhang, Science **335**, 1464 (2012).
[15] Z. Li, J. Li, P. Blaha, and N. Kioussis, Phys. Rev. B **89**, 121117(R) (2014).
[16] C.-J. Kang, H. C. Choi, K. Kim, and B. I. Min, Phys. Rev. Lett. **114**, 166404 (2015).
[17] D. Kasinathan, K. Koepernik, L. H. Tjeng, and M. W. Haverkort, Phys. Rev. B **91**, 195127 (2015).
[18] C.-J. Kang, J. D. Denlinger, J. W. Allen, C.-H. Min, F. Reinert, B. Y. Kang, B. K. Cho, J.-S. Kang, J. H. Shim, and B. I. Min, Phys. Rev. Lett. **116**, 116401 (2016).
[19] P.-Y. Chang, O. Erten, and P. Coleman, Nature Phys. **13**, 794 (2017); arXiv: 1603.03435v1.
[20] T. Takabatake, H. Tanaka, Y. Bando, H. Fujii, S. Nishigori, T. Suzuki, T. Fujita, and G. Kido, Phys. Rev. B **50**, 623 (1994).
[21] T. Ekino, T. Takabatake, H. Tanaka, and H. Fujii, Phys. Rev. Lett. **75**, 4262 (1995).
[22] M. Sera, N. Kobayashi, T. Yoshino, K. Kobayashi, T. Takabatake, G. Nakamoto, and H. Fujii, Phys. Rev. B **55**, 6421 (1997).
[23] H. Kumigashira, T. Takahashi, S. Yoshii, and M. Kasaya, Phys. Rev. Lett. **87**, 067206 (2001).
[24] K. Shimada, K. Kobayashi, T. Narimura, P. Baltzer, H. Namatame, M. Taniguchi, T. Suemitsu, T. Sasakawa, and T. Takabatake, Phys. Rev. B **66**, 155202 (2002).
[25] Y. Kawasaki, M. Izumi, Y. Kishimoto, T. Ohno, H. Tou, Y. Inaoka, M. Sera, and K. Shigetoh, and T. Takabatake, Phys. Rev. B **75**, 094410 (2007).
[26] T. Hiraoka, E. Kinoshita, H. Tanaka, T. Takabatake, H. Fujii, J. Magn. Magn. Mater. **153**, 124 (1996).
[27] As shown in Fig. S1 in the supplement, the cleaved surfaces were flat and large enough for ARPES measurements, but they were not perfectly flat. Hence the energy resolution of the ARPES data is limited by the non-ideally-flat surfaces.
[28] J. D. Denlinger, J. W. Allen, J.-S. Kang, K. Sun, B. I. Min, D.-J. Kim, and Z. Fisk, J. Phys. Soc. Jpn. Conf. Proc. **3**, 017038 (2014).
[29] For $h\nu$ along [100], $h\nu$=122 eV turns out to be close to the ΓYTZ plane in the orthorhombic BZ, and ΓKM plane in the hexagonal BZ. For $h\nu$ along [010], $h\nu$=108 eV is close to the ΓZUX plane in the orthorhombic BZ.
[30] K. Köpernik and H. Eschrig, Phys. Rev. B **59**, 1743 (1999).; I. Opahle, K. Köpernik, and H. Eschrig, Phys. Rev. B **60**, 14035 (1999).; H. Eschrig, K. Köpernik, and I. Chaplygin, J. Solid State Chemistry **176**, 482 (2003).
[31] W. Ku, T. Berlijn, and C.-C. Lee. Phys. Rev. Lett. **104**, 216401 (2010).
[32] P. Blaha, K. Schwarz, G. K. H. Madsen, D. Kvasnicka, J. Luitz, WIEN2k, *An Augmented Plane Wave + Local Orbitals Program for Calculating Crystal Properties*, Karlheinz Schwarz, Techn. Universitat Wien, Austria, (2001), ISBN 3-9501031-1-2.
[33] K. Haule, C.-H. Yee, and K. Kim, Phys. Rev. B **81**, 195107 (2010).
[34] H. C. Choi, B. I. Min, J. H. Shim, K. Haule, and G. Kotliar, Phys. Rev. Lett. **108**, 016402 (2012).
[35] F. Ishii and T. Oguchi, J. Phys. Soc. Jpn. **73**, 145 (2004).
[36] R. Pöttgen, O. Janka, and B. Chevalier, Z. Naturforsch

71, 165 (2016).
[37] Indeed a similar compound of CeRhAs exhibits the structural transition from the hexagonal to orthorhombic structure below T=360 K. See T. Sasakawa, K. Mine, K. Shigetoh, and T. Takabatake, J. Phys. Soc. Jpn. **74**, 3329 (2005).
[38] T. Takabatake, G. Nakamioto, H. Tanaka, Y. Bando, H. Fujii, S. Nishigori, H. Goshima, T. Suzuki, T. Fujita, I. Oguro, T. Hiraoka, and S. K. Malik, Physica B **199-200**, 462 (1994).
[39] See the Supplementary Materials for the Laue patterns, the unfolding scheme of the Ce-only unit cell, and the DMFT band structure of CeRhSb.
[40] In the calculated FS's, slightly deeper initial-state energies (E_i's) are used instead of $E_{\rm F}$ ($E_i \equiv 0$). This is because the shapes of the FS's and those of the constant-energy (CE) surfaces at slightly deeper E_i's are very similar to one another, but the latter exhibit clearer features than the former.
[41] J. J. Yeh and I. Lindau, Atomic Data and Nuclear Data **32**, 1 (1985).
[42] At present, the effect of the band unfolding is not implemented in the DMFT calculations. Hence the different ARPES intensities between the first and second BZ's are not elucidated in the DMFT bands in Figs. 3(d)-(f).
[43] The BZ's superposed on the $h\nu$ maps are calculated by assuming the inner potential V_0=12 eV.
[44] The hole-like character of the FS around U points in the k_a-k_c plane (Fig. 4(b)) is confirmed by the photon-energy dependence of the ARPES spectra. Unpublished data (Seungho Seong, *et al.* (2018)).